

Article

# Robust Two-Layer Model Predictive Control for Full-Bridge NPC Inverter-Based Class-D Voltage Mode Amplifier

Xinwei Wei <sup>1,2</sup>, Hongliang Wang <sup>1,2</sup>, Kangliang Wang <sup>1,2</sup>, Kui Li <sup>1,2</sup>, Minying Li <sup>1</sup> and An Luo <sup>1,2,\*</sup>

<sup>1</sup> Guangdong Zhicheng Champion Group Co., Ltd., Dongguan 523718, China; weixinwei@hnu.edu.cn (X.W.); wanghl123@hnu.edu.cn (H.W.); kangliangwang@hnu.edu.cn (K.W.); kuili@hnu.edu.cn (K.L.); lmy@zhicheng-champion.com (M.L.)

<sup>2</sup> The College of Electrical and Information Engineering, Hunan University, Changsha 410082, China

\* Correspondence: an\_luo@hnu.edu.cn

Received: 8 October 2019; Accepted: 6 November 2019; Published: 14 November 2019



**Abstract:** Finite control set model predictive control (FCS-MPC) is able to handle multiple control objectives and constraints simultaneously with good dynamic performance. However, its industrial application is limited by its high dependence on system model and the huge computational effort. In this paper, a novel robust two-layer MPC (RM-MPC) with strong robustness is proposed for the full-bridge neutral-point clamped (NPC) voltage mode Class-D amplifier (CDA) aiming at this problem. The errors caused by the parameter mismatches or uncertainties of the LC filter and the load current are regarded as lumped disturbance and estimated by the designed Luenberger observer. The robust control can be achieved by compensating the estimated disturbance to the used predictive model. In order to reduce computation of the controller, a two-layer MPC is proposed for the full-bridge NPC inverter with an LC filter. The first layer is used to calculate the optimal output level which minimizes the tracking error of the output voltage. The second layer is used to determine the switching state for the purpose of capacitor voltage balancing. The experimental results show that the lumped model error is observed centrally through only one observer with low complexity. The two-layer MPC further reduced the computation without affecting the dynamic performance.

**Keywords:** model predictive control (MPC); neutral-point clamped (NPC) inverter; disturbance observer; parameter uncertainty; stability analysis

## 1. Introduction

In the area of industrial measurement, testing, and process technology, there exist many applications of power amplifiers in order to generate current and voltage signals of special shape at high power levels. [1,2]. Voltage mode Class-D amplifiers (CDAs), composed of voltage source inverters with LC filters, are used to power voltage-driven loads, such as the piezoelectric ceramic transducer [3] and the electrostrictive transducer [4]. Commonly used inverter topologies in CDAs can be divided into three categories: the half H-bridge inverter [5], the full H-bridge inverter [6–8], and the cascaded H-bridge inverter [1]. However, the used inverter topology in this paper is the full-bridge neutral-point clamped (NPC) inverter, which features lower voltage stress on power semiconductors, lower voltage harmonics, smaller electromagnetic interference compared with the half H-bridge inverter and the full H-bridge inverter [9]. In addition, this topology costs less switch devices compared with the cascaded H-bridge. However, the closed-loop control of the output voltage is still a complex but meaningful issue when this topology and an LC filter are used together as a voltage mode Class-D amplifier. The reason can be stated as follow. First, arbitrary waveforms in a wide band may be required in the CDA [10]. This demand requires the dynamic response of the voltage controller to be fast enough.

Second, load parameters of CDAs may be complex and variable [4–11]. Then the voltage controller is also required to be robust.

In order to achieve output closed-loop control of cascaded H-bridge CDAs, a single PI voltage controller was used in [1]. However, PI gains are required to be turned repeatedly in this method, and the steady state performance and the transient response compromise each other [12]. In [13], a double closed-loop PI controller, whose bandwidth was increased compared with the single PI controller in [1], was used for cascaded H-bridge voltage mode CDAs. Limited by the dynamic performance of the existing linear controllers, nonlinear controllers, such as the sliding mode controller, was proposed in [14,15] for voltage mode CDAs. The sliding mode controller has better dynamic performance, but it suffers from finding out the sliding surface and the existing chattering phenomena.

As another nonlinear controller, model predictive control (MPC) has the advantages of ability to handle multiple control objectives and constraints, simplicity and fast dynamic response, and has been widely concerned and studied in recent years. Moreover, it has been successfully applied to several multilevel inverters. In [16], the finite control set model predictive control (FCS-MPC) was applied for the grid-tied three-phase three-level NPC inverter. In [17], the FCS-MPC was also used to a full-bridge NPC inverter. But in [16,17], the output current or voltage tracking and the capacitor voltage balancing were achieved simultaneously by repeatedly predicting and evaluating the sum of the quadratic terms with weight factors in the cost function, which reflected the two control objectives, respectively. However, the repeated predicting and evaluating the complex cost function costed many computations. In [18], the MPC based on optimal switching sequences was proposed for the full-bridge NPC inverter, which could achieve fixed switching frequency for the switch devices. However, this method failed to balance the capacitor voltage [19]. In [19], a low-complexity MPC was also proposed for the full-bridge NPC rectifier. Although the capacitor voltage balancing could be achieved with unbalanced loads, the fixed switching frequency still limited the dynamic performance of the MPC. In [20,21], the complexity of the MPC algorithm was reduced by employing the multistep MPC for modular multilevel converter (MMC) and cascaded H-bridge inverter. But the dynamic performance would also be affected. In [22,23], only the adjacent voltage vectors or output levels were considered for the FCS-MPC algorithm, and the required computation was reduced greatly. However, both of the dynamic response and the control accuracy would be affected under the condition of load step or reference step for these methods. In [24–27], the process of evaluating the quadratic cost function was regarded as a least square problem, and was proposed to be solved by sphere decoding algorithm or its improved algorithms. But large amount of calculation was still unavoidable for the sphere decoding algorithm.

In addition, because of the high dependence on system model, the effectiveness of the MPC faces enormous challenges when there are errors between the actual system model and the established model. This issue can also be expressed as the robustness of the MPC. The robust MPC has been studied for various power electronic converters, such as three-phase three-level NPC converters [28], three-phase PWM rectifiers [29], flying capacitors inverters [30], and three-phase inverters with LC filters [31,32], etc. In [28], the robustness was achieved by a weighted average process of the measured system variables and the predicted variables. Then the control error caused by the model error could be reduced. However, it failed to deal with the dynamic changes of parameters. In [29], the robust MPC was achieved based on an online disturbance observer. But the influence of the parasitic resistances of the grid-tied inductors were not investigated in the simulation and experiment. In [30], the system robustness was improved based on an adaptive observer. But the variation of the filter inductor was also not included. In [31], the robustness was also achieved based on a disturbance observer. But the load current was obtained by an additional observer, which made the control system more complex. In [32], the output of the three phase inverter prediction model at current control instant was compensated by the modeling error of the last control instant. However, only simulation results were provided, and additional current sensors were required.

In this paper, a robust two-layer MPC is proposed for the full-bridge NPC inverter based CDAs. Based on the designed Luenberger observer, the disturbances caused by both the parameter uncertainties or mismatches of the LC filter and the load current can be centrally estimated and compensated to the prediction model in each control period, which can save computation and avoid the use of load current sensor. Moreover, layered structure is used in the proposed robust MPC, so that the output voltage tracking and the capacitor voltage balancing can be achieved simultaneously and decoupled without affecting the dynamic performance, and the required computation can be further reduced.

The rest of this paper is organized as follows. In Section 2, the discrete mathematical model of the CDA is established. In Section 3, a Luenberger disturbance observer based on Kalman filter is designed to estimate the disturbance caused by the parameter mismatch and the load current. In Section 4, a two-layer MPC for the voltage mode CDA is proposed. Section 5 reports the experiment results. In Section 6, the performance of the proposed robust two-layer MPC is focused on discussion and comparison. And the conclusions are presented in Section 7.

## 2. Modeling of the Voltage Mode Amplifier Using Full-Bridge NPC Inverter

The structure of the full-bridge NPC inverter-based voltage mode Class-D amplifier is shown in Figure 1. The filter inductor is denoted by  $L_f$ , and the filter capacitor is denoted by  $C_f$ . The voltage of  $C_f$  is denoted by  $V_o$ , which is also the final output voltage of the digital amplifier. The current of  $L_f$  is denoted by  $i_f$ , and the final output current of the digital amplifier is denoted by  $i_o$ . Both the defined positive directions of  $i_f$  and  $i_o$  are shown in Figure 1. The output voltage of the full-bridge NPC inverter is denoted by  $V_{ab}$ . The full-bridge NPC inverter consists of two bridges. Each bridge consists of four transistors with four antiparallel freewheeling diodes and two clamping diodes. The dc input is denoted by  $V_{dc}$ , and two identical capacitors  $C_1$  and  $C_2$  are connected in series to obtain two levels of  $V_{dc}/2$  and  $-V_{dc}/2$ . Driving signals of the transistors can be denoted by  $S_{xi}$ .  $x \in \{a, b\}$  denotes legs of the inverter, where  $a$  denotes the left one,  $b$  denotes the right one.  $i \in \{1, 2, 3, 4\}$  denotes the number of transistor in the same bridge. In normal operation,  $S_{a1}$  and  $S_{a3}$  complement each other, and  $S_{a2}$  and  $S_{a4}$  complement each other, too.  $S_{b1}$ ,  $S_{b2}$ ,  $S_{b3}$ , and  $S_{b4}$  also meet this constraint.  $U_{C1}$  and  $U_{C2}$  are used to represent the voltages of capacitors  $C_1$  and  $C_2$ , respectively.  $S$  is defined by  $[S_{a1} S_{a2} S_{a3} S_{a4} S_{b1} S_{b2} S_{b3} S_{b4}]$  and used to denote the switching state of the inverter.  $M$  denotes the output level of the full-bridge NPC inverter. And  $M \in \{-2, -1, 0, 1, 2\}$  is easy to be obtained.

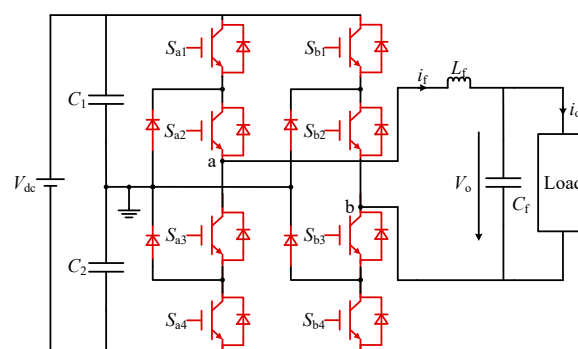


**Figure 1.** The structure of the full-bridge neutral-point clamped (NPC) inverter based voltage mode Class-D amplifier.

Because of the limitation of the complementary driving signals mentioned above, there are only nine effective switching states, which can be denoted by S1–S9. Table 1 shows the relationship between the output level  $M$ , the inductor current  $i_f$ , the change of  $U_{C1}$ , and the nine effective switching states.

**Table 1.** Relationship between  $M$ ,  $i_o$ ,  $U_{C1}$ , and  $S$ .

$M$	$S$	$U_{C1}$	
		$i_o > 0$	$i_o < 0$
2	$S1 = [1\ 1\ 0\ 0\ 0\ 0\ 1\ 1]$	invariant	invariant
1	$S2 = [1\ 1\ 0\ 0\ 0\ 1\ 1\ 0]$	decrease	increase
	$S3 = [0\ 1\ 1\ 0\ 0\ 0\ 1\ 1]$	increase	decrease
0	$S4 = [1\ 1\ 0\ 0\ 1\ 1\ 0\ 0]$	invariant	invariant
	$S5 = [0\ 1\ 1\ 0\ 0\ 1\ 1\ 0]$	invariant	invariant
	$S6 = [0\ 0\ 1\ 1\ 0\ 0\ 1\ 1]$	invariant	invariant
-1	$S7 = [0\ 1\ 1\ 0\ 1\ 1\ 0\ 0]$	increase	decrease
	$S8 = [0\ 0\ 1\ 1\ 0\ 1\ 1\ 0]$	decrease	increase
-2	$S9 = [0\ 0\ 1\ 1\ 1\ 1\ 0\ 0]$	invariant	invariant

Assuming that  $U_{C1}$  and  $U_{C2}$  are well balanced, the differential equation of the full-bridge NPC inverter-based voltage mode amplifier can be obtained as Equation (1) from Figure 1, based on the Kirchoff’s laws of voltage and current.

$$\begin{cases} L_f \frac{di_f}{dt} + V_o = V_{ab} \\ C_f \frac{dV_o}{dt} + i_o = i_f \end{cases} \tag{1}$$

In Equation (1),  $V_{ab}$  can also be represented by the output level of the full-bridge NPC inverter,  $M$ , as shown in Equation (2).

$$V_{ab} = \frac{V_{dc}}{2}M \tag{2}$$

By substituting Equation (2) into Equation (1), Equation (3) can be obtained.

$$\begin{cases} \frac{di_f}{dt} = -\frac{1}{L_f}V_o + \frac{V_{dc}}{2L_f}M \\ \frac{dV_o}{dt} = \frac{1}{C_f}i_f - \frac{1}{C_f}i_o \end{cases} \tag{3}$$

The filter inductor current  $i_f$  and the filter capacitor voltage  $V_o$  can be selected as the state variables of the system, and can be denoted by  $x = [i_f\ V_o]^T$ . Therefore, and the model of the full-bridge NPC inverter based voltage mode amplifier can be transformed into Equation (4),

$$\dot{x} = Ax + B_1M + B_2i_o \tag{4}$$

where  $A = \begin{bmatrix} 0 & -\frac{1}{L_f} \\ \frac{1}{C_f} & 0 \end{bmatrix}$ ,  $B_1 = \begin{bmatrix} \frac{V_{dc}}{2L_f} \\ 0 \end{bmatrix}$ ,  $B_2 = \begin{bmatrix} 0 \\ -\frac{1}{C_f} \end{bmatrix}$ .

For the purpose of digital control, Equation (4) should be discretized. If the sampling period and the control period are denoted as  $T_s$ , the discrete model can be expressed as Equation (5),

$$x(k+1) = A_d x(k) + B_{1d}M(k) + B_{2d}i_o(k) \tag{5}$$

where  $A_d = e^{AT_s}$ ,  $B_{1d} = \int_0^{T_s} e^{A\tau} B_1 d\tau$ ,  $B_{2d} = \int_0^{T_s} e^{A\tau} B_2 d\tau$ ,  $k$  and  $k+1$  represent the  $kT_s$  and  $(k+1)T_s$  instant, respectively.

### 3. Design of the Luenberger Observer for Disturbance Estimation

Luenberger observer adopts a predictor-corrector structure. In the predictor, a predictive model is used to predict the system operation. In the corrector, a feedback signal is compensating to the predictive model to correct the error between the actual system and the used predictive model [29].

In this paper, it is used to estimate and compensate the lumped disturbance caused by the mismatch or uncertainty of the filter parameters and the load current.

### 3.1. Design of the Disturbance Observer

In order to achieve robust MPC, there are two great challenges. The first one is the unknown load current  $i_o$ , because the load current sensor is intentionally avoided. And it will generate large disturbance for the precise control of the output voltage  $V_o$ . The second one is the uncertain parameters of the LC filter. Based on Equations (4) and (5), it can be seen that the parameter matrices  $A_d$ ,  $B_{1d}$ , and  $B_{2d}$  are calculated from  $L_f$  and  $C_f$ , which are the actual parameters of the LC filter. However, the actual parameters  $L_f$  and  $C_f$  may not equal to the nominal parameters  $L_{fn}$  and  $C_{fn}$ , which are used in the controller. The actual parameter of the filter inductor,  $L_f$ , may not be equal to the nominal parameter  $L_{fn}$ , because of several phenomena, such as the magnetic saturation. And the actual parameter of the filter capacitor,  $C_f$ , may also not be equal to the nominal parameter  $C_{fn}$ , because of the unmodeled parasitic resistance and the manufacturing tolerance.

Both of  $L_f$  and  $C_f$  are difficult to obtain accurately in practical engineering. In order to distinguish the discrete model used in the controller from the actual system model, the parameter matrices used in the controller are denoted by  $A_{dn}$ ,  $B_{1dn}$ , and  $B_{2dn}$ , and can be calculated by Equations (6)–(8) based on the nominal parameters  $L_{fn}$  and  $C_{fn}$ , respectively.

$$A_{dn} = e^{A_n T_s} \tag{6}$$

$$B_{1dn} = \int_0^{T_s} e^{A_n \tau} B_{1n} d\tau \tag{7}$$

$$B_{2dn} = \int_0^{T_s} e^{A_n \tau} B_{2n} d\tau \tag{8}$$

$$\text{In (6)–(8), } A_n = \begin{bmatrix} 0 & -\frac{1}{L_{fn}} \\ \frac{1}{C_{fn}} & 0 \end{bmatrix}, B_{1n} = \begin{bmatrix} \frac{V_{dc}}{2L_{fn}} \\ 0 \end{bmatrix}, B_{2n} = \begin{bmatrix} 0 \\ -\frac{1}{C_{fn}} \end{bmatrix}.$$

The relationship between the actual parameter matrices  $A_d$ ,  $B_{1d}$ , and  $B_{2d}$  and the nominal parameter matrices  $A_{dn}$ ,  $B_{1dn}$ , and  $B_{2dn}$  can be shown in Equations (9)–(11),

$$A_d = A_{dn} + \Delta A_d \tag{9}$$

$$B_{1d} = B_{1dn} + \Delta B_{1d} \tag{10}$$

$$B_{2d} = B_{2dn} + \Delta B_{2d} \tag{11}$$

where  $\Delta A_d$ ,  $\Delta B_{1d}$ ,  $\Delta B_{2d}$  denote the model errors caused by the mismatch or uncertainty of the LC filter parameters. Then the discrete system model in Equation (5) can be transformed into Equation (12) by substituting Equations (9)–(11) into (5).

$$x(k + 1) = A_{dn}x(k) + B_{1dn}M(k) + B_{2dn}i_o(k) + \Delta A_d x(k) + \Delta B_{1d}M(k) + \Delta B_{2d}i_o(k) \tag{12}$$

In the right side of Equation (12), there are four uncertain terms. The first one is the third term  $B_{2dn}i_o(k)$ , which is uncertain because of the unknown  $i_o(k)$  in the absence of the load current sensor. The second one and the third one are the fourth term  $\Delta A_d x(k)$  and the fifth term  $\Delta B_{1d}M(k)$ , which are uncertain because of the uncertain matrices  $\Delta A_d$ , and  $\Delta B_{1d}$ . The fourth one is the last term  $\Delta B_{2d}i_o(k)$ , which is uncertain because of both the uncertain matrix  $\Delta B_{2d}$  and the unknown load current  $i_o(k)$ . For the purpose of achieving robust control against the unknown  $i_o(k)$  and the uncertain  $\Delta A_d$ ,  $\Delta B_{1d}$ ,

$\Delta B_{2d}$ , the sum of the four terms is regarded as the lumped disturbance variable  $N(k)$ , as shown in Equation (13).

$$N(k) = B_{2dn}i_o(k) + \Delta A_d x(k) + \Delta B_{1d}M(k) + \Delta B_{2d}i_o(k) \tag{13}$$

The lumped disturbance  $N(k)$  is a two-dimensional variable, and can be expressed as  $N(k) = [N_1(k) \ N_2(k)]^T$ . If both of  $N_1(k)$  and  $N_2(k)$  can be successfully estimated and compensated to the system predictive model based on the nominal parameters in real time, the disturbance-rejection approach can be implemented to achieve robustness against the uncertainty of the filter parameters and the load current  $i_o$ . And this will be still effective even if the system parameters vary during operation, which is regarded as the dynamic parameter variations.

The disturbance variables  $N_1(k)$  and  $N_2(k)$  can be assumed to be constant during each sampling interval [29,31], and they can be extended as the system variables. Then Equation (14) is obtained as,

$$X(k) = \begin{bmatrix} i_f(k) \\ V_o(k) \\ N_1(k) \\ N_2(k) \end{bmatrix} = \begin{bmatrix} A_{dn11} & A_{dn12} & 1 & 0 \\ A_{dn21} & A_{dn22} & 0 & 1 \\ 0 & 0 & 1 & 0 \\ 0 & 0 & 0 & 1 \end{bmatrix} \begin{bmatrix} i_f(k-1) \\ V_o(k-1) \\ N_1(k-1) \\ N_2(k-1) \end{bmatrix} + \begin{bmatrix} B_{1dn11} \\ B_{1dn21} \\ 0 \\ 0 \end{bmatrix} M(k-1) = \Phi X(k-1) + GM(k-1) \tag{14}$$

where  $\Phi = \begin{bmatrix} A_{dn11} & A_{dn12} & 1 & 0 \\ A_{dn21} & A_{dn22} & 0 & 1 \\ 0 & 0 & 1 & 0 \\ 0 & 0 & 0 & 1 \end{bmatrix} = \begin{bmatrix} A_{dn} & 1 \\ 0 & 1 \end{bmatrix}$ ,  $G = \begin{bmatrix} B_{1dn11} \\ B_{1dn21} \\ 0 \\ 0 \end{bmatrix} = \begin{bmatrix} B_{1dn} \\ 0 \end{bmatrix}$ .

And the output equation of the system can be expressed as Equation (15),

$$Y(k) = \begin{bmatrix} i_f(k) \\ V_o(k) \end{bmatrix} = CX(k) \tag{15}$$

where  $C = \begin{bmatrix} 1 & 0 & 0 & 0 \\ 0 & 1 & 0 & 0 \end{bmatrix}$ .

Based on Equations (14) and (15), a discrete observer can be constructed as shown in Equation (16),

$$\hat{X}(k) = \Phi \hat{X}(k-1) + GM(k-1) + L(Y(k-1) - \hat{Y}(k-1)) = \Phi \hat{X}(k-1) + GM(k-1) + LC(X(k-1) - \hat{X}(k-1)) \tag{16}$$

where  $\hat{X}(k)$  and  $\hat{X}(k-1)$  respectively denote the estimated value of  $X(k)$  and  $X(k-1)$ , and  $L$  denotes the gain matrix.  $M(k-1)$  denotes the output level of the full-bridge NPC inverter in the  $(k-1)$ th control period, which is obtained by the proposed two-layer MPC in the  $(k-1)$ th control period.

$\hat{N}(k)$  can be used to denote the estimated value of  $N(k)$ , and it can be calculated by Equation (17).

$$\hat{N}(k) = \begin{bmatrix} \hat{N}_1(k) \\ \hat{N}_2(k) \end{bmatrix} = \begin{bmatrix} 0 & 0 & 1 & 1 \end{bmatrix} \begin{bmatrix} \hat{i}_f(k) \\ \hat{V}_o(k) \\ \hat{N}_1(k) \\ \hat{N}_2(k) \end{bmatrix} \tag{17}$$

### 3.2. Parameter Design

The Kalman filter is a commonly used method to optimally estimate the state of a dynamic system from a series of imperfect noisy measurements, especially in presence of uncertainties [31]. In this paper, the designed observer can be regarded as a discrete Kalman filter to calculate the observer gain matrix  $L$ .

As an optimal recursive data processing algorithm, the discrete Kalman filter can perform cyclic calculation according to the following five steps in each control period.

The first step is to calculate the prior state estimate value  $\hat{X}_k^-$  based on Equation (18).

$$\hat{X}_k^- = \Phi \hat{X}(k-1) + GM(k-1) \quad (18)$$

The second step is to calculate the priori estimate error covariance matrix  $P_k^-$  based on Equation (19),

$$P_k^- = \Phi P_{k-1} \Phi^T + Q \quad (19)$$

where  $Q$  is the given process noise covariance matrix, and  $P_{k-1}$  is the posteriori estimate error covariance matrix in the last control period.

The third step is to calculate the observer gain matrix  $L$  based on Equation (20),

$$L = P_k^- C^T (C P_k^- C^T + R)^{-1} \quad (20)$$

where  $R$  is the given measurement noise covariance matrix.

The fourth step is to update the estimated state variable  $\hat{X}(k)$  based on Equation (21).

$$\hat{X}(k) = \hat{X}_k^- + L(Y(k) - C\hat{X}_k^-) \quad (21)$$

The fifth step is to calculate the posteriori estimate error covariance matrix  $P_k$  based on Equation (22).

$$P_k = (I - LC)P_k^- \quad (22)$$

where  $I$  denotes the identity matrix.

The first step and the second step can be collectively referred to as the prediction link of the discrete Kalman filter. And the last three steps can be collectively referred to as the correction link of the discrete Kalman filter.

The stability of the designed discrete Kalman filter has been proved by [31,33], and will not be discussed here.

*Remark:* The performance of the designed state observer is determined by the given matrix  $Q$  and  $R$ . The larger  $Q$  is, the faster the observed values converge to their actual value, but too fast convergence speed will lead to noise interference. The smaller  $R$  is, the less noise interference, but the slower convergence rate. Therefore,  $Q$  and  $R$  should be adjusted synthetically to achieve the tradeoff between convergence speed and noise suppression.

#### 4. Two-Layer Model Predictive Control

The basic control objectives of the voltage CDA using full-bridge NPC inverter include two terms: (1) output voltage tracking; (2) capacitor voltage balancing. Traditional FCS-MPC (TFCS-MPC) requires repeated predictions and evaluations for each effective switching state, and the one which minimizes the cost function is selected as the optimal control option. Thus when it is applied to the full-bridge NPC inverter, there will be nine candidate switching states. And this places large computational burden on the digital controllers when a small control period is required.

Therefore, a two-layer MPC for the cascaded full-bridge NPC voltage mode amplifier is proposed in this paper, which is much simpler than TFCS-MPC without affecting the dynamic performance. And the proposed two-layer MPC decouples the two control objectives, which also allows the two control objectives to be achieved simultaneously without weight factors. The structure of the proposed two-layer MPC is shown in Figure 2, where the first layer is used to calculate the optimal output level for the purpose of achieving the first control objective, the second layer is used to determine the switching state for the purpose of achieving the second control objective.

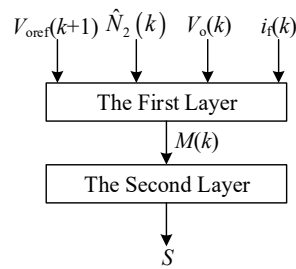


**Figure 2.** The structure of the proposed two-layer model predictive control (MPC).

#### 4.1. The First Layer

The reference of the output voltage can be denoted by  $V_{oref}$ , which is also the voltage signal to be amplified. In this system, the cost function corresponding to level  $h$  can be defined as  $J(h)$  in Equation (23),

$$J(h) = |V_{oref}(k + 1) - V_{oh}(k + 1)|, \quad h \in H = \{-2n, -2n + 1, \dots, 0, \dots, 2n - 1, 2n\} \quad (23)$$

where  $V_{oh}(k+1)$  denotes the output current at  $(k+1)T_s$  instant when  $h$  is selected in the  $k$ th control period.

Based on Equations (12) and (13),  $V_{oh}(k+1)$  can be predicted as given in Equation (24).

$$V_{oh}(k + 1) = A_{dn21}i_f(k) + A_{dn22}V_o(k) + B_{1dn21}M(k) + N_2(k) \quad (24)$$

In Equation (24),  $N_2(k)$  cannot be obtained because it is determined by the uncertain model errors and the unknown load current  $i_o$  without configured load current sensor. However, the designed Luenburger observer can successfully estimate  $N_2(k)$  to  $\hat{N}_2(k)$ , then we are allowed to replace  $N_2(k)$  with  $\hat{N}_2(k)$ . Thus Equation (24) can be improved to Equation (25).

$$V_{oh}(k + 1) = A_{dn21}i_f(k) + A_{dn22}V_o(k) + B_{1dn21}M(k) + \hat{N}_2(k) \quad (25)$$

Another function,  $J_1(h)$ , with the output level  $h$  as its independent variable can be defined by Equation (26).

$$J_1(h) = V_{oh}(k + 1) - V_{oref}(k + 1) = A_{dn21}i_f(k) + A_{dn22}V_o(k) + B_{1dn21}M(k) + N_2(k) - V_{oref}(k + 1) \quad (26)$$

The relationship between  $J_1(h)$  and  $h$  will be linear if  $h$  is supposed to be continuous. For the convenience of expression, another variable,  $h_{sol}$  is defined as the solution of  $J_1(h) = 0$ , and can be calculated as Equation (27).

$$h_{sol} = \frac{V_{oref}(k + 1) - A_{dn21}i_f(k) - A_{dn22}V_o(k) - N_2(k)}{B_{1dn21}} \quad (27)$$

Because of  $J(h) = |J_1(h)| \geq 0$ , the optimal output level  $M(k)$ , which minimizes  $J(h)$ , must be equal to the integer nearest to  $h_{sol}$ . Thus the optimal output level  $M(k)$  is allowed to be directly obtained by Equation (28),

$$M(k) = \operatorname{argmin}_{h \in H} |J_1(h)| = \operatorname{round}(h|_{J_1(h)=0}) \quad (28)$$

where  $\operatorname{round}(x)$  denotes the rounding function, which is equal to the integer nearest to  $x$ .

In order to avoid the case that the result of Equation (28) does not belong to  $H$ , Equation (29) is also required after Equation (28).

$$M(k) = \begin{cases} 2, & M(k) > 2 \\ M(k), & -2 \leq M(k) \leq 2 \\ -2, & M(k) < -2 \end{cases} \quad (29)$$

Thus the cost function is evaluated only once, which greatly reduces the computational burden.

#### 4.2. The Second Layer

The second layer is used to determine the switching state to achieve capacitor voltage balancing. At the same time, the switching action times should also be considered when the switching state is determined, because there are multiple switching states to be selected if level  $-1$ ,  $0$ , or  $1$  is required.

In steady-state operation, the full-bridge NPC inverter is generally switched between adjacent levels. Thus the output level will be switched between  $2$ ,  $1$ , and  $0$  when  $M(k) > 0$ . Table 2 shows the number of switching actions when the three levels are switched between each other. According to Table 2, if the submodule output level is  $2$ , the switching state can only select  $S1$ . If the submodule output level is  $1$ , in order to achieve the purpose of capacitor voltage balance,  $S2$  should be selected when the signs of  $i_o$  and  $\Delta U_C$  are the same, while  $S3$  should be selected when they are opposite, considering the result of Table 1. If the submodule output level is  $0$ , the switching state can only select  $S5$ , in order to minimize the switching actions when level  $0$  and level  $1$  are switched between each other.

**Table 2.** Switching actions when the output level switching between  $2$ ,  $1$ , and  $0$ .

Switching Level	Switching State	Action Times
2 and 1	S1 and S2	2
	S1 and S3	2
1 and 0	S2 and S4	2
	S2 and S5	2
	S2 and S6	6
	S3 and S4	6
	S3 and S5	2
	S3 and S6	2
2 and 0	S1 and S4	4
	S1 and S5	4
	S1 and S6	4

Similar analysis can be done when  $M(k) < 0$  and the following conclusions can be drawn. If the submodule output level is  $-2$ ,  $S9$  is selected. If the submodule output level is  $-1$ ,  $S8$  is selected when the signs of  $i_o$  and  $\Delta U_C$  are the same, while  $S7$  is selected when the signs of  $i_o$  and  $\Delta U_C$  are opposite. If the submodule output level is  $0$ ,  $S5$  is selected.

Figure 3 shows the flow chart of the switching state selection process. The parallel structure of the middle and lower layer control shows that they are more suitable for implementation by a FPGA.

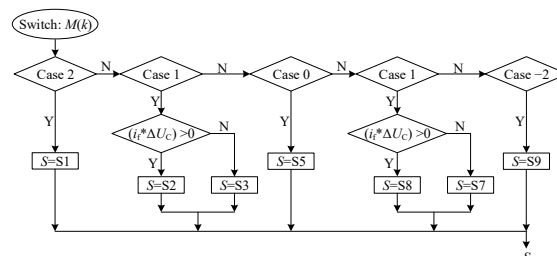


**Figure 3.** The flowchart of the switching state selection process.

### 5. Experimental Verification

In order to verify the feasibility and validity of the proposed robust multilayer MPC applied to the full-bridge NPC voltage-mode digital power amplifier, a  $2$  kW experimental prototype with a  $50$  Hz– $800$  Hz output band is built in the laboratory as shown in Figure 4. The actual value  $L_f$  of the filter

inductor used is 2 mH, and the actual value  $C_f$  of the filter capacitor used is 10  $\mu$ F. The voltage of the dc input,  $V_{dc}$ , is 300 V, so that two voltage levels of 150 V and  $-150$  V can be obtained. The capacitance of those two capacitors  $C_1$  and  $C_2$  is 1070  $\mu$ F. The control frequency is set to be 100 kHz, which means that the sample period is set to be 10  $\mu$ s. The high control frequency is used because wide range output frequency and high precision out voltage are required. Thus the maximum switching frequency of the used switch devices is 50 kHz. In fact, the designed digital power amplifier uses SGH80N60UFD type fast IGBT and DSE130–60; a type fast recovery diode, whose maximum switching frequency can be up to 100 kHz.



**Figure 4.** The designed 2 kW experiment prototype.

### 5.1. Steady State Performance

In order to study the steady state performance of the proposed RM-MPC, the output voltage reference  $V_{oref}$  is set to a sine wave with an 800 Hz frequency and a 200 V root-mean-square (RMS) value, which may be widely used in underwater electroacoustic transduction system. The load is set to a 20  $\Omega$  resistor. The experiment results are shown in Figure 5, where (a) shows the waveforms of  $V_o$  and its reference  $V_{oref}$ , (b) shows the waveform of the estimated value of  $N_1$ , (c) shows the waveform of the estimated value of  $N_2$ , (d) shows the waveforms of the two capacitor voltages in the dc side.

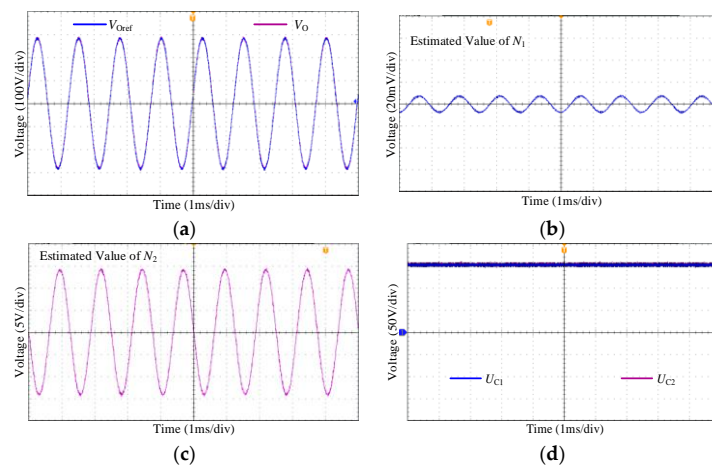


**Figure 5.** Steady state experiment results. (a) Waveforms of  $V_o$  and  $V_{oref}$ ; (b) Waveform of the estimated value of  $N_1$ ; (c) Waveform of the estimated value of  $N_2$ ; (d) Waveforms of capacitor voltages.

It can be seen that the output voltage is accurately tracked with a 0.52% total harmonics distortion (THD). At the same time, the two capacitor voltages in the dc side are well balanced. In addition, the disturbance variables  $N_1$  and  $N_2$  are successfully estimated with little noises. In this way, the proposed RM-MPC shows good steady state performance.

### 5.2. Dynamic Performance

In order to study the dynamic performance of the proposed RM-MPC, the output voltage reference  $V_{oref}$  is set to a sine wave with an 50 Hz frequency and a 100V RMS value for initialization. However, the RMS value of the desired sine wave steps to 200 V at  $t = 0.05$  s. And the load is still set to a 20  $\Omega$

resistor. The experiment results are shown in Figure 6, where (a) shows the waveforms of  $V_o$  and its reference  $V_{oref}$ , (b) shows the waveform of the estimated value of  $N_1$ , (c) shows the waveform of the estimated value of  $N_2$ , (d) shows the waveforms of the two capacitor voltages in the dc side.

It can be seen that the output voltage tracks the step variation of its reference quickly, and the tracking error is reduced to 1 V within 0.54 ms. Besides, the two capacitor voltages in the dc side are also well balanced during transient variation. Thus, the fast dynamic performance of the proposed multilayer MPC is verified. Moreover, Figure 6b,c shows that the estimated values of  $N_1$  and  $N_2$  change quickly with the step variation of  $V_{oref}$ , so that the fast dynamic performance of the designed Luenberger observer is also verified.

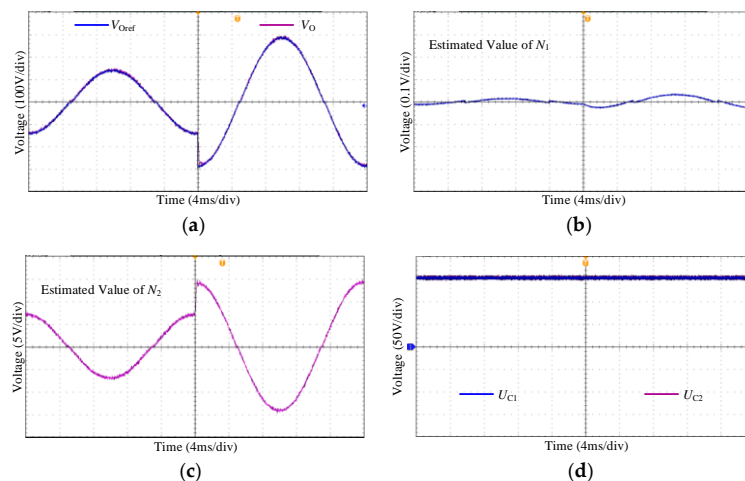


**Figure 6.** Dynamic experiment results. (a) Waveforms of  $V_o$  and  $V_{oref}$ ; (b) waveform of the estimated value of  $N_1$ ; (c) waveform of the estimated value of  $N_2$ ; (d) waveforms of capacitor voltages.

### 5.3. Robust Performance

In order to study the robust performance of the proposed RM-MPC, two groups of experiments are carried out, where the output voltage reference  $V_{oref}$  is set to a sine wave with an 50 Hz frequency and a 200 V RMS value, and the load is also set to a 20  $\Omega$  resistor. However, in the first group, the inductance value used in the controller is set to 1 mH, and the capacitance value used in the controller is set to 5  $\mu$ F, which means that there are  $-50\%$  parameter mismatch. In the second group, the inductance value used in the controller is set to 3 mH, and the capacitance value used in the controller is set to 15  $\mu$ F, which means that there are  $+50\%$  parameter mismatch.

The results of the first group experiment are shown in Figure 7, where (a) shows the waveforms of  $V_o$  and its reference  $V_{oref}$ , (b) shows the waveform of the estimated value of  $N_1$ , (c) shows the waveform of the estimated value of  $N_2$ , (d) shows the waveforms of the two capacitor voltages in the dc side. And the results of the second group experiment are shown in Figure 8.

It can be seen that the good tracking effect of the output voltage are maintained with the help of the designed Luenberger observer, even if there are  $\pm 50\%$  parameter mismatches. Furthermore, the well capacitor voltage balancing is also achieved against the parameter mismatches. Thus the strong robustness is also verified by the experiment results.

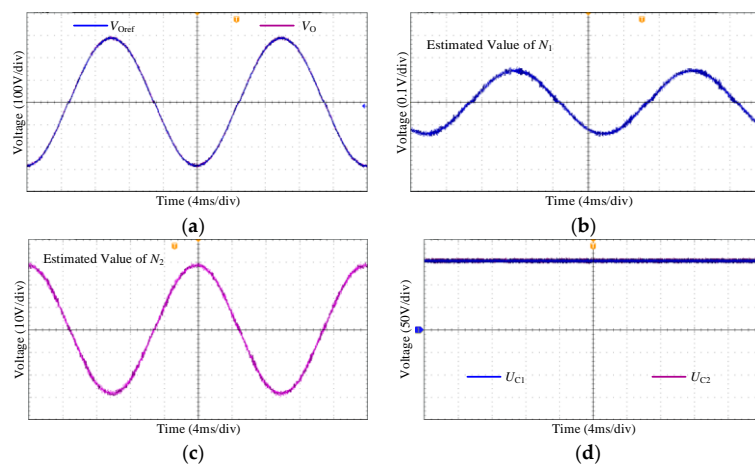


**Figure 7.** Robustness experiment results with  $-50\%$  parameter mismatch. (a) Waveforms of  $V_O$  and  $V_{oref}$ ; (b) waveform of the estimated value of  $N_1$ ; (c) waveform of the estimated value of  $N_2$ ; (d) waveforms of capacitor voltages.

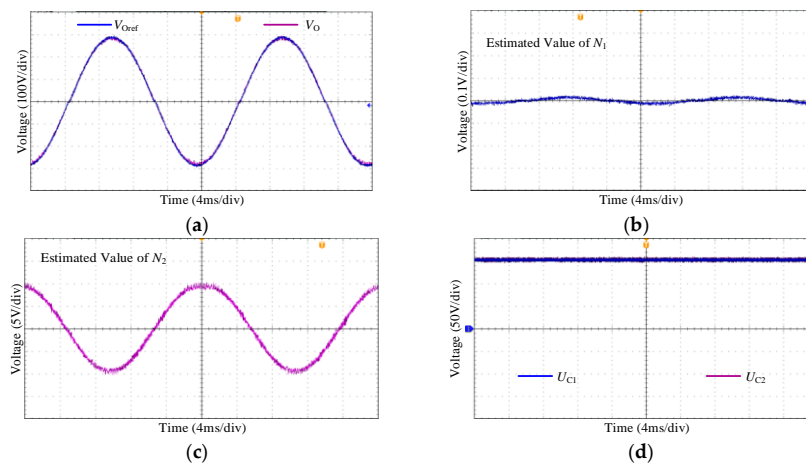


**Figure 8.** Robustness experiment results with  $+50\%$  parameter mismatch. (a) Waveforms of  $V_O$  and  $V_{oref}$ ; (b) waveform of the estimated value of  $N_1$ ; (c) waveform of the estimated value of  $N_2$ ; (d) waveforms of capacitor voltages.

## 6. Discussion

In Section 3.1, it can be seen that all the uncertain terms in Equation (12) can be divided into three categories, which are the ones related to the load current, the ones related to the uncertain parameters, and the ones related to both the load current and the uncertain parameters. In Sections 5.1 and 5.2, there are no parameter uncertainties or mismatches, then the designed observer only estimates the uncertain term related to the load current. In this way, the observer operates as a load current observer, and the two subsections of 5.1 and 5.2 focus on the steady-state and dynamic performance of the designed observer and the proposed two-layer MPC. In Section 5.3, parameter uncertainties exist, and the designed observer estimates the sum of all the uncertain terms. Thus Section 5.3 focuses on the robustness performance against the parameter mismatches of the LC filter.

Compared with the dual observers used method in [31] and the additional current sensors based method in [32], only one observer is used to observer all the uncertain terms caused by the parameter uncertainties and the load current in a centralized way. This not only improves the system robustness against both the parameter uncertainties of the filter inductor and the filter capacitor, but also avoids the use of additional load current sensors and observers. And this also leads to a reduction in both the amount of calculation and the economic cost for the hardware configuration. In addition, the layered

structure of the proposed MPC further reduces the computation. It can be inferred that the proposed robust MPC can also be extended to general inverters with LC filters, which are widely used in distributed generation systems, energy storage systems, and uninterruptible power supplies.

## 7. Conclusions

In this paper, a robust multilayer MPC, which can achieve decoupling control of the output voltage and capacitor voltage balancing simultaneously in different layers against the parameter uncertainties or mismatches of the LC filter, is proposed for the full-bridge NPC inverter-based CDAs. The errors caused by the parameter mismatches or uncertainties of the LC filter and the load current are regarded as lumped disturbance and estimated by the designed Luenberger observer. Based on the estimated disturbance, a two-layer MPC is proposed, where the output voltage tracking and the capacitor voltage balancing are achieved in the first layer and the second layer, respectively. Finally, the steady state performance, the dynamic performance and the robust performance are verified on the designed 2 kW experiment prototype.

Compared with existing methods, the proposed robust two-layer MPC uses only one observer to observe the lumped disturbance caused by the parameter mismatch and the load current, which simplifies the control system and reduces the calculation of the system. The layered structure further reduces the computation without affecting the dynamic performance of the MPC. However, the control delay is not considered, which may affect the control effect and calls for further research.

**Author Contributions:** Conceptualization, X.W.; formal analysis, A.L.; funding acquisition, M.L.; investigation, X.W.; methodology, A.L.; project administration, M.L.; software, K.L.; validation, K.W.; writing—original draft, X.W.; writing—review and editing, H.W. and A.L.

**Funding:** The Program for Guangdong Introducing Innovative and Entrepreneurial Teams: 2017ZT07G23; Research on High-power and High-efficiency Electro-acoustic Transduction Mechanism and Control Method: 51837005; Research on Topology, Passive Current Sharing Mechanism and Control for Multiphase Resonant Converter with Coupled Resonant Tank: 51977069.

**Conflicts of Interest:** The authors declare no conflict of interest.

## References

1. Ertl, H.; Kolar, J.W.; Zach, F.C. Analysis of a multilevel multicell switch-mode power amplifier employing the “flying-battery” concept. *IEEE Trans. Ind. Electron.* **2002**, *49*, 816–823. [[CrossRef](#)]
2. Zhou, J.; Deng, Z.; Liu, C.; Li, K.; He, J. Current ripple analysis of five-phase six-leg switching power amplifiers for magnetic bearing with one-cycle control. In Proceedings of the 2016 19th International Conference on Electrical Machines and Systems (ICEMS), Chiba, Japan, 13–16 November 2016; pp. 1–6.
3. Agbossou, K.; Dion, J.L.; Carignan, S.; Abdelkrim, M.; Cheriti, A. Class D amplifier for a power piezoelectric load. *IEEE Trans. Ultrason. Ferroelectr. Freq. Control.* **2000**, *47*, 1036–1041. [[CrossRef](#)] [[PubMed](#)]
4. Kagawa, Y.; Gladwell, G.M.L. Finite Element Analysis of Flexure-Type Vibrators with Electrostrictive Transducers. *IEEE Trans. Sonics Ultrason.* **1970**, *17*, 41–48. [[CrossRef](#)]
5. Colli-Menchi, A.I.; Torres, J.; Sánchez-Sinencio, E.A. Feed-Forward Power-Supply Noise Cancellation Technique for Single-Ended Class-D Audio Amplifiers. *IEEE J. Solid-State Circuits* **2014**, *49*, 718–728. [[CrossRef](#)]
6. Fang, J.; Ren, Y. Self-adaptive phase-lead compensation based on unsymmetrical current sampling resistance network for magnetic bearing switching power amplifiers. *IEEE Trans. Ind. Electron.* **2012**, *59*, 1218–1227. [[CrossRef](#)]
7. Wang, X.; Zhao, Z.; Li, K.; Chen, K.; Liu, F. Analysis of the Steady-State Current Ripple in Multileg Class-D Power Amplifiers Under Inductance Mismatches. *IEEE Trans. Power Electron.* **2019**, *34*, 3646–3657. [[CrossRef](#)]
8. Hung, T.; Rode, J.; Larson, L.; Asbeck, P. H-Bridge Class-D Power Amplifiers for Digital Pulse Modulation Transmitters. In Proceedings of the 2007 IEEE/MTT-S International Microwave Symposium, Honolulu, HI, USA, 3–8 June 2007; pp. 1091–1094.

9. Song, W.; Ma, J.; Feng, L.Z.X. Deadbeat Predictive Power Control of Single-Phase Three-Level Neutral-Point-Clamped Converters Using Space-Vector Modulation for Electric Railway Traction. *IEEE Trans. Power Electron.* **2016**, *31*, 721–732. [[CrossRef](#)]
10. Morozov, K.A.; Scussel, K.F.; Coryer, M.W.M.J. The new development of the autonomous sources for ocean acoustic navigation, tomography and communications. In Proceedings of the IEEE OCEANS, Anchorage, AK, USA, 19–22 September 2017; pp. 1–8.
11. Sherman, C.; Butler, J. *Transducers and Arrays for Underwater Sound*; Springer: New York, NY, USA, 2007.
12. Kakosimos, P.; Abu-Rub, H. Predictive control of a Grid-Tied cascaded full-bridge NPC inverter for reducing high-frequency common-mode voltage components. *IEEE Trans. Ind. Inf.* **2018**, *14*, 2385–2394. [[CrossRef](#)]
13. Dong, M.; Zhang, Y.; Li, M.X.J. Multilevel dual closed-loop controlling Class-D power amplifier with FPGA. *Int. Conf. Control. Eng. Comm. Tech.* **2012**, 421–425.
14. Yu, S.; Tseng, M. Optimal control of a nine-level Class-D audio amplifier using sliding-mode quantization. *IEEE Trans. Ind. Electron.* **2011**, *58*, 3069–3076. [[CrossRef](#)]
15. Zhang, Y.; Meng, Q.; Li, Y.; Cai, L. A high-efficiency cascaded multilevel class-D amplifier with FPGA based on sliding mode control. In Proceedings of the 2010 3rd International Symposium on Systems and Control in Aeronautics and Astronautics (ISSCAA 2010), Harbin, China, 8–10 June 2010; pp. 86–90.
16. Hamdi, M.; Hamouda, M.; Al-Haddad, L.S.K. FCS-MPC for grid-tied three-phase three-level NPC inverter with experimental validation. In Proceedings of the International Conference on Green Energy Conversion Systems (GECS), Hammamet, Tunisia, 23–25 March 2017; pp. 1–6.
17. Stolze, P.; Kramkowski, M.; Mouton, T.; Kennel, M.T.R. Increasing the performance of finite-set model predictive control by oversampling. In Proceedings of the IEEE Conference on Innovative Engineering Technologies, Cape Town, South Africa, 25–28 February 2013; pp. 551–556.
18. Vazquez, S.; Aguilera, R.P.; Acuna, P.; Pou, J.; Leon, J.I.; Franquelo, L.G.; Agelidis, V.G. Model Predictive Control for Single-Phase NPC Converters Based on Optimal Switching Sequences. *IEEE Trans. Ind. Electron.* **2016**, *63*, 7533–7541. [[CrossRef](#)]
19. Ma, J.; Song, W.; Wang, X.; Feng, F.B.X. Low-Complexity Model Predictive Control of Single-Phase Three-Level Rectifiers with Unbalanced Load. *IEEE Trans. Power Electron.* **2018**, *33*, 8936–8947. [[CrossRef](#)]
20. Baidya, R.; Acuna, R.A.P. Multistep model predictive control for cascaded H-bridge inverters: Formulation and analysis. *IEEE Trans. Power Electron.* **2018**, *33*, 876–886. [[CrossRef](#)]
21. Guo, P.; He, Z.; Yue, Y.; Xu, Q.; Huang, X.; Chen, Y.; Luo, A. A novel two-stage model predictive control for modular multilevel converter with reduced computation. *IEEE Trans. Ind. Electron.* **2019**, *66*, 2410–2422. [[CrossRef](#)]
22. Cortes, P.; Wilson, A.; Kouuro, S.; Rodriguez, J.; Abu-Rub, H. Model predictive control of multilevel cascaded H-bridge inverters. *IEEE Trans. Ind. Electron.* **2010**, *57*, 2691–2699. [[CrossRef](#)]
23. Gong, Z.; Dai, P.; Yuan, X.; Guo, X.W.G. Design and experimental evaluation of fast model predictive control for modular multilevel converters. *IEEE Trans. Ind. Electron.* **2016**, *63*, 3845–3856. [[CrossRef](#)]
24. Karamanakos, P.; Kennel, T.G.R. Reformulation of the long horizon direct model predictive control problem to reduce the computational effort. In Proceedings of the IEEE Energy Conversion Congress and Exposition, Pittsburgh, PA, USA, 14–18 September 2014; pp. 3512–3519.
25. Karamanakos, P.; Kennel, T.G.R. A computationally efficient model predictive control strategy for linear systems with integer inputs. *IEEE Trans. Control. Syst. Technol.* **2016**, *24*, 1463–1471. [[CrossRef](#)]
26. Karamanakos, P.; Kennel, T.G.R. Constrained long-horizon direct model predictive control for power electronics. In Proceedings of the Energy Conversion Congress & Exposition, Milwaukee, WI, USA, 18–22 September 2016; pp. 1–8.
27. Karamanakos, P.; Mouton, T.G.T. Computationally efficient sphere decoding for long-horizon direct model predictive control. In Proceedings of the Energy Conversion Congress & Exposition, Milwaukee, WI, USA, 18–22 September 2016; pp. 18–22.
28. Zhang, Z.; Li, Z.; Kazmierkowski, M.; Kennel, J.R.R. Robust predictive control of three-level NPC back-to-back power converter PMSG wind turbine systems with revised predictions. *IEEE Trans. Power Electron.* **2018**, *33*, 9588–9598. [[CrossRef](#)]
29. Xia, C.; Wang, M.; Liu, Z.S.T. Robust model predictive current control of three-phase voltage source PWM rectifier with online disturbance observation. *IEEE Trans. Ind. Inf.* **2012**, *8*, 459–471. [[CrossRef](#)]

30. Ghanes, M.; Trabelsi, M.; Ben-Brahim, H.A.L. Robust adaptive observer-based model predictive control for multilevel flying capacitors inverter. *IEEE Trans. Ind. Electron.* **2016**, *63*, 7876–7886. [[CrossRef](#)]
31. Nguyen, H.; Kim, E.; Kim, I.; Jung, H.C.J. Model predictive control with modulated optimal vector for a three-phase inverter with an LC filter. *IEEE Trans. Power Electron.* **2018**, *33*, 2690–2703. [[CrossRef](#)]
32. Shen, K.; Zhang, J. Modeling error compensation in FCS-MPC of a three-phase inverter. In Proceedings of the 2012 IEEE International Conference on Power Electronics, Drives & Energy Systems (PEDES), Bengaluru, India, 16–19 December 2012; pp. 1–6.
33. Jazwinski, A. *Stochastic Processes and Filtering Theory*; Academic Press: Pittsburgh, PA, USA, 1970.



© 2019 by the authors. Licensee MDPI, Basel, Switzerland. This article is an open access article distributed under the terms and conditions of the Creative Commons Attribution (CC BY) license (<http://creativecommons.org/licenses/by/4.0/>).